Title
Ion Dynamics and Polarizations in a Simulated Nanopore under Alternating Current Controls

Journal
ACS Electrochemistry, 1(12)

ISSN
2997-0571

Authors
Yang, Zicheng
D'Antona, Nick
Boettcher, Shannon W
et al.

Publication Date
2025-12-04

DOI
10.1021/acselectrochem.5c00284

Ion Dynamics and Polarizations in Simulated Nanopore under Alternating Current Controls

Zicheng Yang,[1] Nick D'Antona,[2] Shannon W. Boettcher,[2] Niya Sa[1*]

1. Department of Chemistry, University of Massachusetts – Boston, Boston, Massachusetts 02125, United States
2. Department of Chemistry & Biomolecular Engineering and Department of Chemistry, University of California, Berkeley, California 94720, United States; Energy Storage and Distributed Resources Division, Lawrence Berkeley National Laboratory, Berkeley, California, 94720, United States

*Corresponding Author: Niya Sa, Email: Niya.Sa@umb.edu

ABSTRACT

Understanding the ion transport through nanopores provides a central basis in advancing the design of molecular sensors or preparation of biomimetic systems based on nanopores. Here we report a continuum modeling approach that introduces an alternating current (AC) field to investigate the competition between a surface-charge dominated electromigration process under a frequency induced ion dynamics at nanoscales. We highlight a transition from a surface-charge-dominated effect, where electric double layer (EDL) impacts prevail, to bulk-like ion dynamics as pore dimensions approach the microscale. The results reveal that rapid electromigration dominates ion distribution at a millisecond timescale, generating transient, non-equilibrium concentration profiles. In contrast, lower frequency perturbations enable diffusion to equilibrate ion distributions within each cycle, establishing periodic quasi-steady states. The findings from this work highlight the interplay of the ion selectivity and distribution by exploiting the dynamic competition between electromigration and diffusion in oscillating bias systems.

TOC FIGURE

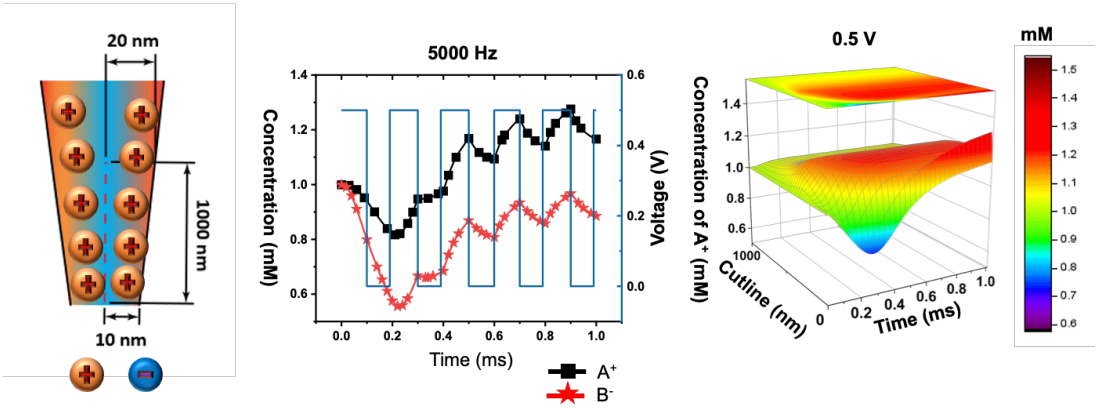

KEYWORDS: alternating current ion dynamics, ion concentration polarization, nanopore, Poisson-Nernst-Planck theory

INTRODUCTION

Inspired by biological nanochannels, nanopores are model structures that serve as critical platforms for studying the physics and electrochemistry of nanoconfined solvent and ions. Nanopore systems have been widely applied in various applications including water desalination,[1,2] and chemical and biological separations.[3–5] In particular, understanding ion transport is critical for advancing ionic or molecular sensors,[6–13] with nanopore sensing platforms playing a pivotal role in DNA sequencing, drug delivery and sensing *etc*.[14,15] These platforms also provide key insights into drug-protein interactions.[16,17] The ion transport is regulated by external physical fields such as electricfields.[18,19] In many of these applications, a direct current (DC) is used to electrophoretically

drive ions through the confined space in nanopore device, while the changes in ionic conductance serve as detection signal for translocating molecules, ions, or polymers.[20–24]

Alternating current (AC) has distinct advantages over DC in systems involving dynamic control of ion transport.[25,26] For instance, AC is employed in ion ratchet systems for gel electrophoresis and electronic switching in logic circuits,[27] demonstrating its versatility in manipulating charged particles. Unlike DC systems, AC stimulation can even be generated through photocurrent-driven processes, such as via proton pumping across membranes, enabling unique biohybrid applications.[28] A critical challenge in nanopore-based DNA sequencing arises from the inherent noise in resistive-pulse signals, which obscures molecular-level details during translocation events and the fundamental limitations of conventional DC-based sensing methods.[29–32]A survey of the literature reveals limited studies on the alternating current (AC) controlled ion translocation. AC voltage modulation has been used to study conductance fluctuations of DNA translocation in nanopores, revealing a complex interplay between the predominantly diffusive motion and field effects.[33] Resistance-based detection of DNA and small molecules in solution have been used to leverage ion transport through arrays of nanopores.[34–36] Non-linear voltage sweeps—enabled by AC stimulation—can accelerate ion transport by rapidly dissipating accumulated charges within nanopores.[37] This contrasts sharply with DC-driven systems, where stagnant charge layers often hinder mass transport.

The use of AC control has advantages compared to the conventional DC controls to understand translocation through nanopore systems. It is believed that the AC bias with zero offset is expected to place a lower net driving force to translocate for highly charged biomolecules as compared with DC, consequently easing the control of molecule translocation in a single cycle.[38,39] However, the physical mechanisms governing ion transport in nanopores under electric fields involve complex

interactions between the surface charge effects and the constrained volume, making direct study of the nanopore physics challenging. As such, there is relatively little that is known about the behavior of nanopores under the influence of an alternating electric field,[40,41] which indicates a need for understanding the time-dependent ion dynamics and polarizations. For instance, the surface charge effect of nanopores prominently influences ion transport, especially at low ionic strengths due to the overlap of electrical double layers. Such overlapping induces an excess of counterions to maintain electroneutrality and create permselectivity.[42] This permselectivity, however, is just one facet of the ionic behavior within nanopores. The ionic current rectification effect (ICR), observed as a non-linear current-voltage relationship, is another prominent feature. ICR often arises from the induced ionic concentration polarization with asymmetric ion concentration profiles at the nanopore entrance and exit.[43,44] Ion current rectification and electroosmotic flow in asymmetrically charged conical nanopores can be tuned by voltage scan rate, pressure, and surface charge, enabling diode-like behavior and novel nanoscale transport phenomena with potential applications in sensing and fluid control.[45,46]

Finite-element simulation provides a path to understanding these interactions by building model systems and modulating key variables to assess their importance in ion transport behavior in nanopore systems transparently governed by established physics. Ion transport in a nanopore subject to an alternating electric field results in a complex and dynamic interplay between migratory and diffusive transport mechanisms. Excess surface-charge on the inner pore wall induces localized fields that occupy a significant fraction of the area of the nanopore (overlapping electric double layers), establishing ionic concentration gradients that transverse the pore length. Simultaneously, the application of high-frequency AC voltage perturbation induces longitudinal (along the length of the nanopore) electrostatic potential gradients that drive ion migration through the pore.

At somewhat longer timescales, concentration gradients in the nanopore introduce a significant diffusive transport mode. As nanopore dimensions expand from the tens to hundreds of nanometers in diameter, ion transport is dominated by the AC field rather than the surface-charge dominated ion distribution associated with the nanoconfinement and overlapping double layers.

Using finite- element simulations, we investigated these coupled phenomena within nanopores at different diameters subject to varying AC voltage frequencies. We found that at millisecond timescales, ion-transport dynamics are governed by the transient formation of electric double layers (EDLs) at the surface of the nanopore, which dominates the early-stage ion redistribution at the nanopore. As operational timescales extend, high-frequency regimes induce dynamic, non-equilibrium concentration shifts within the nanopore, driven by the competition between electromigration and diffusion. Conversely, at low-frequency modulation, ion transport shifts to a quasi-steady state regime, where periodic equilibration between field-driven migration and diffusive relaxation establishes predictable, oscillatory concentration profiles. Findings from this simulation study offer important implications for the operation and design of nanostructured materials to regulate ion transport in devices. The influence of the altered electric potential modulates the surface charge density dominating mass transport, and such control must be carefully considered to achieve the desired device performance for ion separation and applications.

SIMULATION METHODS

Simulation of ionic transport with potential gradient was conducted by solving couple diffusion (Fick's second law) and migration process (Poisson-Nernst-Planck) with finite-element method using COMSOL Multiphysics 6.1. The 2D model is shown in **Figure 1** and schematic plot in **Figure S1**. The boundary conditions were set considering the surface charge at the nano channel area,

potential, the initial concentration, and constant concentration. The length of nanopore is 1000 nm with diameter 20 nm and 200 nm. The surface charge density is -0.001 C/m^2 at the wall of nanopore. The fine mesh (0.1 nm) applied at the inner nanopore to describe the effect of electrical double layers. The coarse mesh (0.5 nm) was chosen for the reservoirs area to decrease the computer memory cost during calculations. Binary ions of cation A^+ and anion B^- are considered in electrolyte. The uniform salt concentration is 1 mM at bulk with the related transport governed by parameters including diffusion coefficient (1 $\mu m^2/s$) and permittivity of water (78.5 F/m).

The voltage is applied at the top edge (AB) in **Figure 1** of the reservoir which is the square wave function with 0.5 V amplitude, 1 Hz and 5000 Hz frequency, 0.5 duty cycle. The mathematical expression of the square wave function is:

$$E(t) = 0.5\mathrm{sgn}(\sin(2\pi f t)) \tag{1}$$

Applying sgn operator to the sine wave clips the continuous waveform to just its sign. Whenever the sine is positive, $E(t) = +0.5$; whenever it is negative, $E(t) = 0$. In the model the total time is 5 period of each frequency, and the time step is the t_{tot} /100.

The Poisson-Nernst-Planck equation determines the potential distribution in the solution by the electric potential from applied and surface charge density from material.

$$\nabla \cdot (\varepsilon \nabla \Phi) = -\rho \tag{2}$$

where ε is the dielectric constant, Φ is the electrostatic potential, and ρ is the charge density applied at wall of nanopore as -0.001 C/m^2. The Nernst-Planck equation is :

$$\frac{\partial c_i}{\partial t} + \nabla \cdot J = 0 \tag{3}$$

Where c_i is the concentration of ion and the function of time (t) and position (x). J is the flux and it neglect convection and only consider the diffusion and migration in the dilute limit there they can be cleanly decoupled in the transport equation.

$$J = -D\nabla c_i - \frac{D_i z_i F}{RT} c_i \nabla \Phi \quad (4)$$

D is the diffusion coefficient, set to 10^{-12} m^2/s represents high-viscosity aqueous systems (e.g., gel, tissues), c is the concentration of i ion, F is the faraday constant, z_i is the valence of charge ion, R is gas constant Φ is the electric potential.

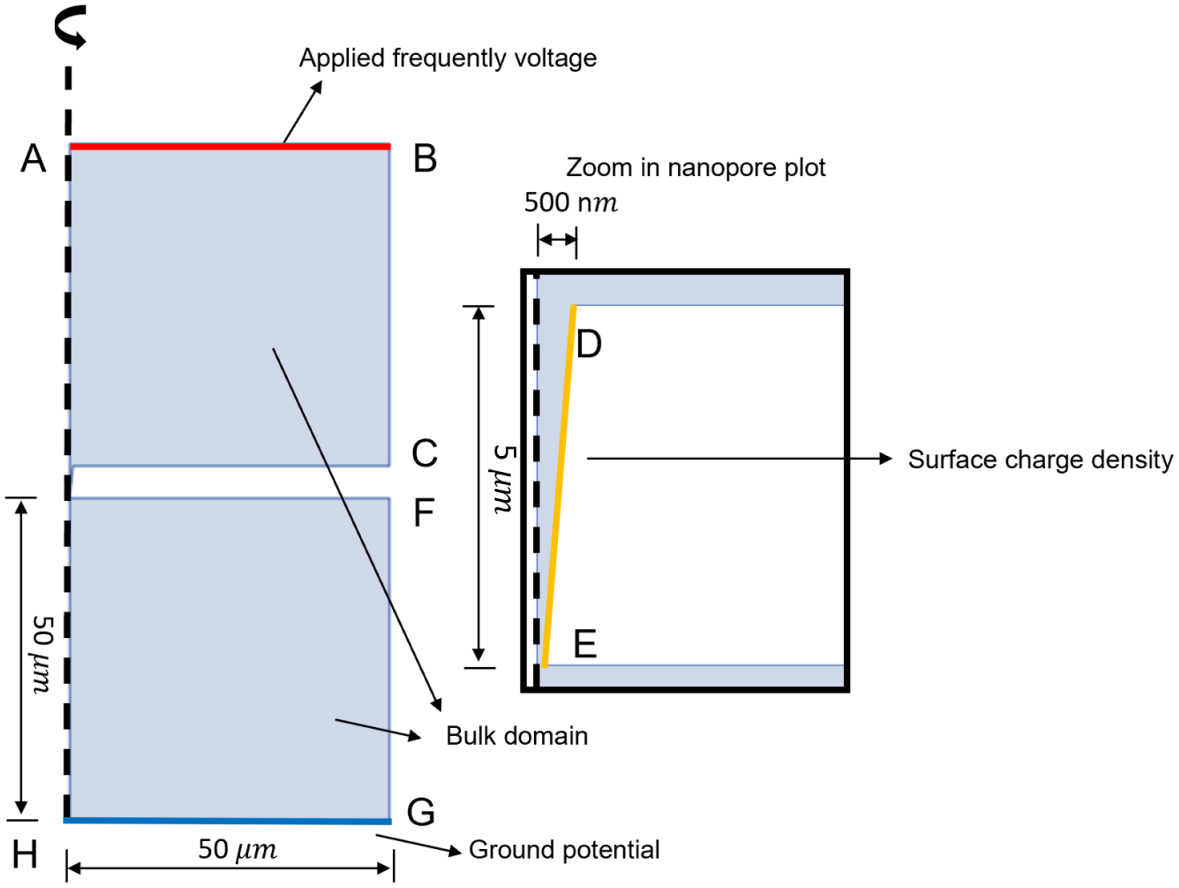

Figure 1. Scheme of the 2D axis symmetric geometry used in simulations. A zoomed in cone region is shown on the right. The ground potential is placed on boundary H-G and the applied

potential is on boundary A-B. Dash line represents the cutline of the model as well as the symmetry axis of the model. The initial concentration of cation and anion is 1 mM.

RESULTS AND DISCUSSION

Non-Equilibrium Ion Dynamics via Electromigration-Diffusion Competition at High Frequency Fields: Results from **Figure 2** depict the transient cation and anion concentration profiles in a conical nanopore (20 nm diameter) under a 5 kHz pulsed electric field revealing a dynamic interplay between surface charge effects and an altered electric field-driven ion migration. Within the first 0.2 ms, cation concentration at the nanopore tip (0 nm cutline: point at 0 nm in the center of the pore) drops sharply from 1 mM to 0.8 mM (**Figure 2a**), driven by ion concentration polarization (ICP) induced by the negatively surface charge density (-0.001 C/m^2, referenced with the experimentally measured surface charge density on the Silica Si-OH surface, where 1mC/m^2 is roughly corresponding to 6000 charge/μm^2).[47] Critically, the initial configuration of the simulation is such that the surface charge on the inner walls of the nanopore induced a double layer formation at $t > 0$. The small radius of the nanopore tip and low electrolyte concentration (1 mM) results in a transient depletion of the ion concentration in the tip region. This can be seen more clearly in the graphs of the A^+ concentration profile at 0.1 ms and 0.45 ms (**Figure 2b**), where the concentration profile of A^+ cations is not uniform along the entire length of the nanopore wall as one might expect (given the constant surface charge density).

This is because the volume of the tip region is small enough that there are not enough total ions present in that region of solution to compensate the total excess charge on the inner wall of the tip. This results in a transient depletion of the concentration of A^+ at the tip at short times (~0.1 ms) which is then replenished by longer range transport of A^+ ions from further up the shaft of the

nanopore at slightly longer times (~0.4 ms). At 0.4 ms, the establishment of the electric double layer along the inner walls of the nanopore is complete and the concentration of A^+ is higher than its bulk value due to their overlap in the tip region. Thus, in the range of 0 to 0.4 ms, the concentration profile does not follow the voltage perturbation (**Figure 2a**), as surface charge in the nanopore dominates ion transport at early times. By $t \geq 0.4$ ms, however, the surface effects have reached equilibrium, and the time-dependent concentration profiles are controlled by migration induced by the longitudinal AC electric potential distribution. Concentration at the tip rises during active pulses (0.4-0.5 ms, 0.6-0.7 ms) and declines during off-phases (0.5-0.6 ms, 0.7-0.8 ms), reflecting non-equilibrium electromigration-diffusion competition.

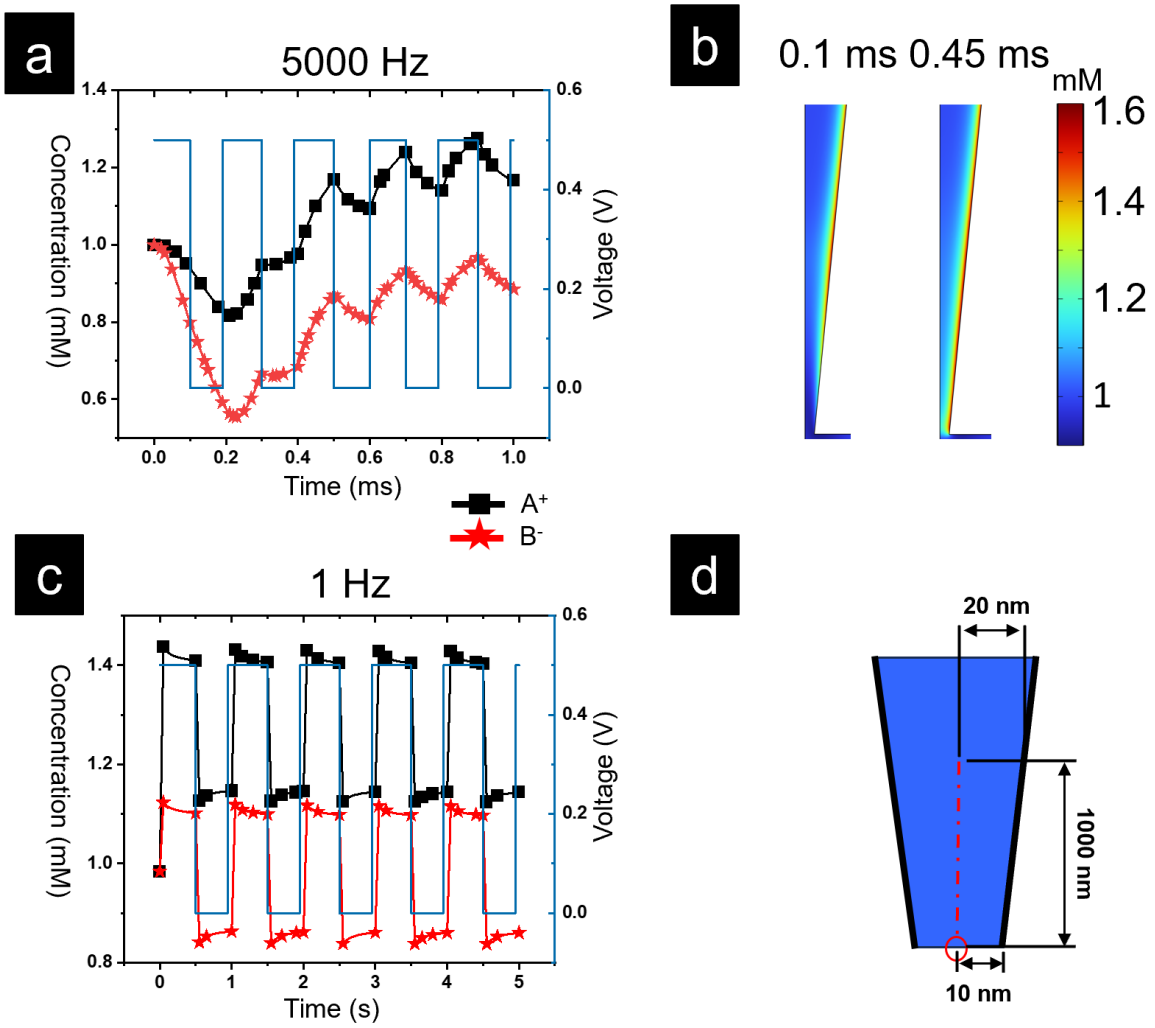

Figure 2. (a) The concentration of cation A^+ (black) and anion B^- (red) (the data points are the averaged representation) as a function of time at the tip of the nanopore (20 nm in diameter) over-layed with the 5000 Hz voltage perturbation (blue). (b) The concentration profile of cation A+ in the nanopore cone at 0.1 ms and 0.45 ms under the 5000 Hz perturbation. (c) Identical graph to (a) but at a 1 Hz voltage perturbation. (d) schematic of nanopore section, with cutline shown as the dash line at the center of the geometry. The simulated ion distribution in panel a and panel c are shown at the center of the red-circle point. Nanopore diameter of 20 nm with cone angle of 1.1º. The highlighted red circle at the center of the nanopore tip is where data from panel a and c are

simulated. The diffusion coefficients are $D_A = 1 \times 10^{-12} m^2/s$ and $D_B = 1 \times 10^{-12} m^2/s$. The total number of data points simulated is 111 and this is applied for both (a) and (b).

Quasi-Equilibrium Ion Dynamics via Electromigration-Diffusion Competition at Low Frequency Fields: Simulation revealed a frequency-dependent electric field transition of ion concentration distribution driven from surface-charge-dominated to the external field-governed ion dynamics. At t < 0.2 ms, the formation of the EDL delays the system's response to the high frequency field, where the surface charge redistributes ions to screen the local electric potential: a phenomenon consistent with nanoscale EDL overlap effects.[45] However, once the EDL stabilizes (t ≥ 0.4 ms), the rapid 5000 Hz pulses (0.2 ms cycle) forces ions into a non-equilibrium state. The confinement of gradients to <500 nm (**Figure 2a**) further underscores the role of pore geometry in focusing field effects: the conical tip amplifies local field intensity, enhancing electromigration within the nanoscale while leaving bulk-like zones unaffected in **Figure S2**. In the longer-duration simulation results (5 ms) shown in **Figure S3**, the cation concentration exhibits rapid oscillations following the 5000 Hz electric field, while the difference between maximum concentration values during field activation approaches zero. The ratcheting up of concentrations is correlated to the AC electric field for both cation and anion with increasing time. **Figure 2d** presents a schematic of the nanopore section, with the red-circle point indicating the location at a 20 nm diameter where the data shown in Figures 2a and 2c were calculated. **Figure 2c** illustrates the cation and anion concentration dynamics at the tip (0 nm cutline) of a conical nanopore under a 1 Hz pulsed electric field, spanning a 5 s timeframe. The pulsed field, applied in 0.5 s intervals (0-0.5 s, 1-1.5 s, etc.), induces periodic cation accumulation and depletion phases. During each active pulse, the electric field drives cations toward the negatively charged density tip, generating a sharp concentration

peak (1.43 mM) within 0.1 s. Conversely, anions are repelled, forming a depletion zone. When the field is turned off (0.5-1 s, 1.5-2 s *etc*.), cation concentration decays to 1.12 mM at the tip due to diffusion-driven relaxation, while anions gradually recover toward equilibrium. This cyclic behavior produces five distinct concentration waves, reflecting the interplay of electromigration and diffusion at low frequency. And the concentration distribution shows an oscillation wave along the 1000 nm cut line in nanopore with electric field in **Figure S4**.

The quasi-steady state is established within each pulse cycle, enabled by the slow 1 Hz frequency. During field-on phases electromigration dominates, rapidly accumulating cations at the tip. However, unlike the high-frequency case (**Figure 2a**), the 0.5 s pulse duration allows sufficient time for diffusion to partially counteract electromigration, leading to a slight decline in cation concentration (from 1.43 mM to 1.42 mM) even before the field is turned off. The extended off-phase (0.5 s) further permits diffusion to redistribute ions, reducing tip concentration to 1. 12 mM before the next pulse begins. These observations show that ion transport at low frequencies is dominated by bulk diffusion and migration rather than surface charge effects, which are only present at short times in the high frequency regime.

The thickening and overlap of EDLs during the field-on phases (**Figure 2a**) highlights the role of surface charge in ion transport. The conical geometry amplifies EDL overlap at the tip, enhancing counterion screening,[44] while the pulsed field periodically disrupts this equilibrium. The depletion of anion during active pulses (**Figure 2c**) further confirms surface-charge-governed selectivity, as co-ions are expelled from the EDL region. These dynamics resemble voltage-gate ion channels,[46] where periodic fields regulate ionic access. However, the quasi-steady concentration recovery during off-phases contrasts with high-frequency regimes (**Figure 2a**), where diffusion cannot keep pace with rapid field changes.

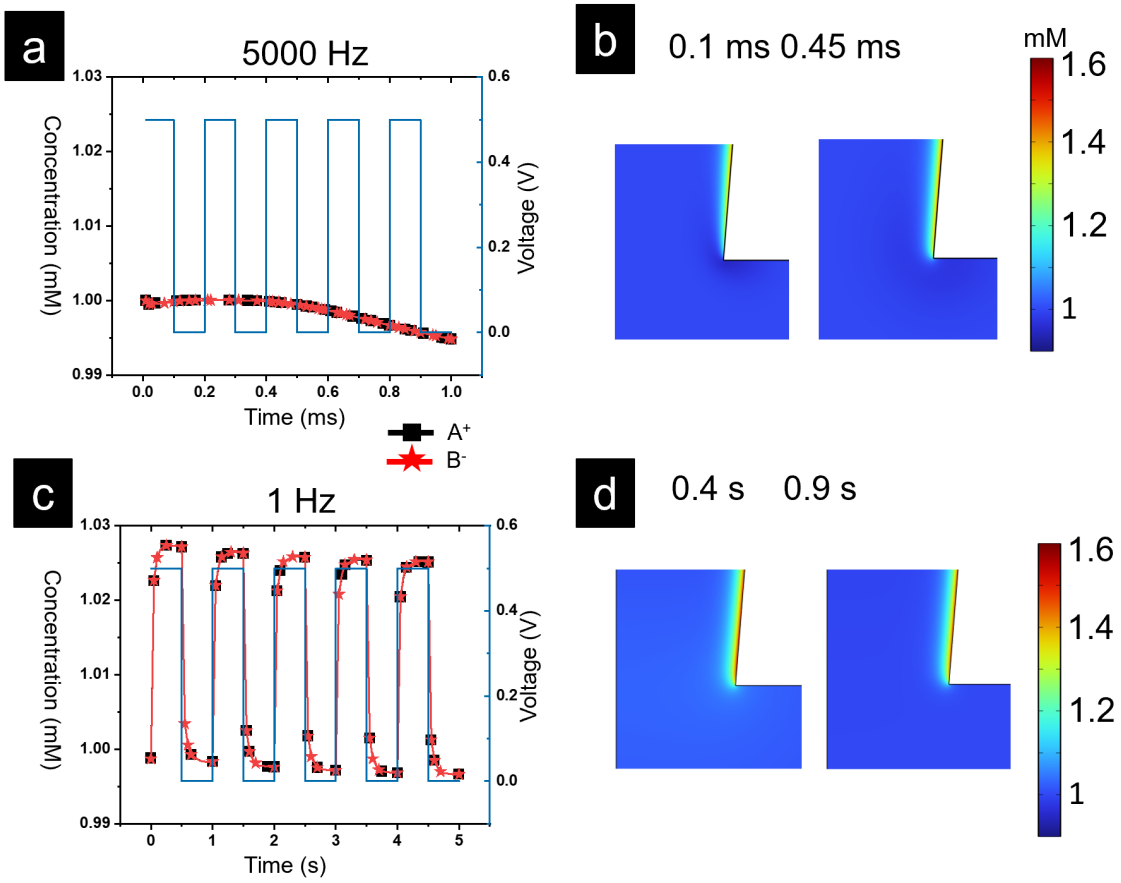

Figure 3. (a) The concentration of cation A^+ (black) and anion B^- (red) as a function of time subject to a 5000 Hz perturbation; (b) Snapshots of cation A^+ concentration profile at 0.1 ms and 0.45 ms at a 5000 Hz voltage perturbation; (c) Concentration profile of cation A^+ (black) and anion B^- (red) as a function of time subject to a 1 Hz perturbation; (d) Snapshots of cation A^+ concentration profile at 0.4 s and 0.9 sat 1 Hz perturbation. Nanopore opening is 200 nm in diameter at all panels. The diffusion coefficients are $D_A = 1 \times 10^{-12} m^2/s$ and $D_B = 1 \times 10^{-12} m^2/s$. For panel a&c, similar cutline as presented in Figure 2d is used here to extract the concentration profile. The number of data points for (a) and (b) is 110.

Pore Dimension to Ion Transport and Dynamics at Frequency-Dependent Field: The above-mentioned electromigration-diffusion competition at high frequency fields is further investigated under the control of pore size. **Figure 3a** shows the effect of increasing the pore size to 200 nm in diameter at the tip, where at a frequency of 5000 Hz the concentration of ions in the pore is nominally insensitive to the external applied voltage within time. Unlike in the case of smaller nanopore (**Figure 2**), where the double layer extends approximately 10 nm into the bulk solution from the wall, the time dependent formation and redistribution of the double layer does not substantially impact the concentration of ions ~100 nm away towards the middle of the nanopore. Consequently, the rate of ions transport into and out of the nanopore tip remains comparable as the pore dimension increased to 200 nm in diameter and no obvious ion depletion or enhancement is seen. A small decrease in the ion concentration with time is still seen, which may be attributed to the ion redistribution near the surface forming the double layer. **Figure 3b** shows the nearly identical A^+ concentration profiles in the middle of nanopore at 0.1 ms and 0.45 ms, while the formation of double layers is clearly visible near at the inner wall tips in the graphs. **Figure 3c** shows the concentration of cation A^+ and anion B^- at the tip and center of the pore as a function of time under a lower frequency voltage perturbation of 1 Hz. The concentration of both cations and anions increases and decreases with the 1 Hz perturbation to the same extent, whereas the concentration of anions was relatively lower when the pore size was 20 nm in diameter across (**Figure 3c**). This effect again arises from the double layer overlap in the 20 nm size (in diameter) creating an asymmetric transport limitation on ion transport. The accumulation of cations in the pore tip facilitates their transport relative to anions, whereas double layer overlap does not affect the equilibrium ion distribution in the large 200 nm in diameter pores and thus does not have an asymmetric effect on the transport of one ion relative to another in center. Figure 3d similarly shows that, under a 1 Hz

external voltage signal, the extent of the pore-wall double layer is small relative to the pore opening. This observation supports the claim that the symmetric ion transport in the center of a large nanopore arises from the absence of overlapping double layers at the pore walls. The concentration distribution of cation along the 1000 nm cut line in nanopore with the AC electric field is shown in **Figure S5**. The complete set of datapoints simulated for ion concentrations is shown in Figure S6.

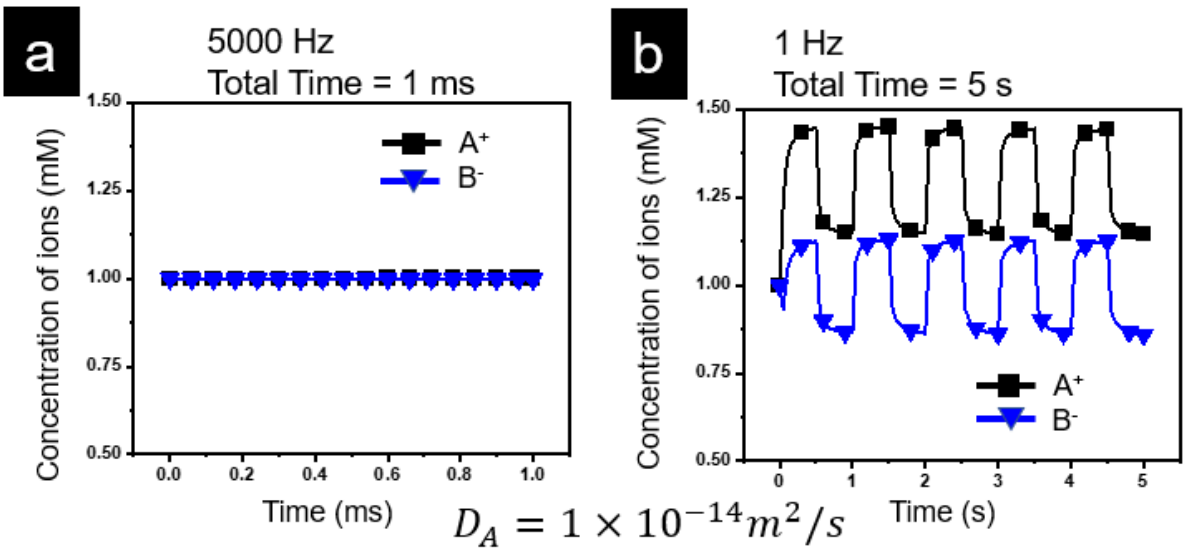

Figure 4. Concentration plots of ions with diffusion coefficients $D_A = 1 \times 10^{-14} m^2/s$ and $D_B = 1 \times 10^{-15} m^2/s$. Panel (a) displays the scenario at an applied frequency of voltage field at 5000 Hz over a total duration of 1 ms, while panel (b) shows the results at 1 Hz over 5 s. The concentration of ions is within a cone shape (20 nm in diameter) nanopore at the cut point 0 nm.

Ion Diffusion Coefficient and its Correlation to the Ion Concentration Distribution at Altered Field: A decreased of ion diffusion coefficient (as compared with **Figure 3**) has been applied to investigate the ion concentration distribution at the AC controls in a 20 nm in diameter

nanopore, results are presented in **Figure 4**. Herein, we adopt benchmark values of the cation diffusion coefficient of $D_A = 1 \times 10^{-14}\ m^2/s$ and the anion diffusion coefficient of $D_B = 1 \times 10^{-15}\ m^2/s$ to represent scenarios with mismatched ion mobilities. Such disparity in diffusion coefficients has been experimentally observed in systems including biomolecule sensing with polymer backbones, ionogels, and solvated zwitterions. [10,48] At 5000 Hz, the concentrations of both ions are unaffected by the external voltage in the time range 0-1 msec. Despite the small size of the pore relative to the spatial extent of the pore wall double layer (once formed), the 100-1000x decrease in diffusion coefficients increases the length of time required for it to be established. At 1 Hz (**Figure 4b**), cation A^+ exhibits periodic oscillations, peaking at ~1.45 mM during field-on phases (0-0.5 s) and decaying to ~1.2 mM during off-phases. The anion B^- shows the same trend, increasing to ~1.1 mM under the field and recovering to 0.8 mM post-pulse. Because the time range observed in this case is within the order of seconds rather than milliseconds, the formation of the pore wall double layer is relatively fast, and thus the concentration profile is similar to what's seen in **Figure 2c**, though they differ in the time scale to approach to the maximum concentration.

The central insight is that the degree of the ion diffusion coefficient can transition the system from a regime where the ionic concentrations in the pore rapidly respond to the AC fields induced nonequilibrium charge distributions, versus the sluggish transport that are insensitive to rapid changes in the electric field. At 1 Hz, the long pulse duration (0.5 s) allows a slow replacement of B^- to partially redistribute via electromigration and diffusion. Lowered ion mobility results in a gradual accumulation of ions during field-on intervals (e.g., 0–0.5 s, 1–1.5 s), suggesting that reduced transport delay the attainment of a quasi-equilibrium state under an identical electric field condition. At 5000 Hz, however, neither ion adjusts to the short 0.2 ms pulses. For A^+ and B^-, the

diffusion timescale exceeds the pulse cycle, which results in ion transport that is diffusion limited. The difference of diffusion coefficient for A^+ and B^- suggests that smaller ions partially adapt to rapid fields, while bulky ion species exhibit a slow adaption to field changes.[49] Notably, the ion concentration profile displays consistent oscillations at a 1 Hz frequency, suggesting a dynamic ion transport interaction with the alternating electric field (**Figure S7**). Conversely, at a 5000 Hz frequency, the concentration profile appears relatively flat, indicating that the rapid alterations on (off) in the electric field do not significantly impact ions concentration distribution due to the slow movement of ions within the 20 nm in diameter cone shape nanopore. Such distinct response highlights how the ion diffusion coefficient governs the timescale over which ions redistribute in response to varying frequencies of the applied electric field. The interplay between the diffusion coefficient and the field frequency dictates whether ion transport is dominated by dynamic electromigration or mitigated by diffusive relaxation. Notably, the liquid junction potential (LJP) is neglected in the simulation model, which disregards the natural asymmetry that arises when ion mobilities differ. Omitting the LJP may artificially impose symmetry in ion transport that does not reflect physical reality.

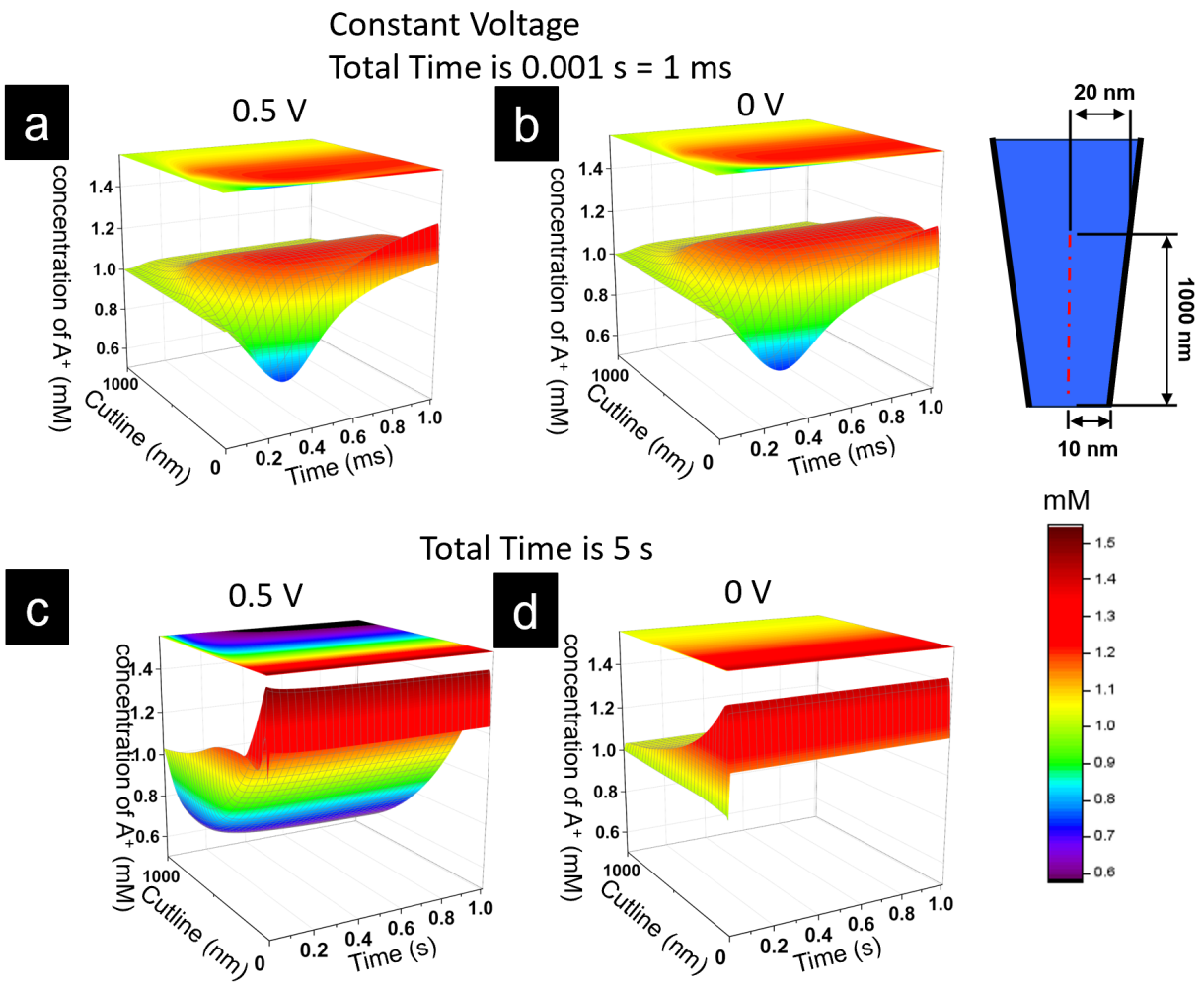

Figure 5. The concentration of A^+ ion as a function of time with cone shape (20 nm in diameter) nanopore and cut line length of 1000 nm. The applied electric potential and total time are, respectively, (a) 0.5 V, 1 ms, (b) 0 V, 1 ms (c), 0.5 V, 5 s, and (d) 0 V, 5 s.

Effect of Constant Electric Field on the Ion Distribution. The system response to time varying electric fields has thus far revealed that the pore wall double layer formation is important for explaining concentration vs time plots at different frequency controls. The time dependence of the double layer formation was examined independently from applied AC voltage by recording concentration profiles as a function of time under constant voltage.

Figure 5 presents 3d concentration profiles of cation A^+ (z axis with color projection on the top) in a conical nanopore (20 nm diameter, cutline: 1000 nm-y axis) under now *constant* electric field conditions versus time (x axis). Panels (a) and (c) represent the system's response under an applied voltage of 0.5 V, while panels (b) and (d) depict the system with no applied voltage. At 0.5 V (Figure 5a), the concentration of cation sharply decreases from 1 mM (bulk) to 0.75 mM within the first 0.3 msec due to pore wall double layer formation depleting the tip region of ion. Subsequently, electrophoretic migration and pore wall double layer overlap drives an increase to 1.3 mM at 1 ms near the 0 nm cutline.

Without the electric field (Figure 5b), the concentration profile similarly drops to 0.75 mM initially but recovers to 1.2 mM at 1 ms, exceeding the bulk concentration—a phenomenon attributed to the exclusion-enrichment effect from double layer at nanoconfinement.[50] At an applied DC voltage of 0.5 V for 5s (Figure 5c), the concentration profile establishes a maximum value of 1.47 mM near the tip. Conversely, while in the absence of an electric field (Figure 5d), the concentration profile of A^+ is stabilized at 1.4 mM (0 nm cutline), the difference between these two being the effect of field driven migration along the pore length, leading to additional cation accumulation in the tip.

While the Poisson-Nernst-Planck simulations capture key information about AC-driven ion dynamics in nanopores, several limitations need consideration. First, the lack of electroosmotic flow (via Navier-Stokes equations) neglects potential fluid motion, which could accelerate ion redistribution at high frequencies. Second, surface charge density was treated as uniform and constant, while real systems exhibit complex and dynamic situations. The assumption of a fixed charge density ($\sigma = -0.001$ C/m²) overlooks dynamic charge modulation under electric fields, which could alter EDL formation timescales. Finally, our model ignores the ion-ion correlations and steric

effects, which become significant at high concentrated solutions. These simplifications were necessary to isolate electromigration-diffusion competition but may limit quantitative accuracy in systems where convection or charge nonlinearities dominate.

CONCLUSIONS

This study offers a new mechanistic understanding of the dynamic competition between electromigration and diffusion by successfully coupling a time-dependent Poisson equation with Nernst-Planck transport under alternating electric field boundary conditions. Results reveal a rapid electromigration dominated ion distribution at high frequency controls, generating transient, non-equilibrium concentration profiles. In contrast, lower frequency perturbations enable diffusion to equilibrate ion distributions, establishing periodic quasi-steady states. Findings from this work highlight the interplay of the ion selectivity and distribution by exploiting the dynamic competition between electromigration and diffusion. This simulation study offers important implications for the operation and design of nanostructured materials to regulate ion transport in devices. In particular, AC modulation provides a powerful means to tune ion selectivity, suppress concentration polarization, and control transient accumulation or depletion of ions within confined geometries. Such control is directly relevant for nanopore sensors, where alternating potentials may reduce baseline drift and noise while enhancing temporal resolution of analyte translocation events. The influence of the altered electric potential modulates the surface charge dominated mass transport at confined geometries, and such control must be carefully considered to achieve the desired device performance for ion separation and applications. Insights from this study establish AC modulation as a powerful and tunable strategy for designing next-generation nanopore sensors, ion-selective devices.

ASSOCIATED CONTENT

Supporting Information

The Supporting Information is available free of charge. The Supporting Information includes 3D ion concentration dynamics profiles, a 1000 nm cut-line analysis along the nanopore center, and time-dependent behavior under an alternating electric field. Additionally, the 2D axisymmetric geometry model used for simulations is provided.

AUTHOR INFORMATION

Corresponding Author

Niya Sa – *Department of Chemistry, University of Massachusetts – Boston, Boston, Massachusetts 02125, United States*

ORCID (0000-0003-4656-5851)

Email: Niya.Sa@umb.edu

Authors

Zicheng Yang – *Department of Chemistry, University of Massachusetts – Boston, Boston, Massachusetts 02125, United States*

Email: Zicheng.Yang001@umb.edu

Nick D'Antona – *Department of Chemistry & Biomolecular Engineering and Department of Chemistry, University of California, Berkeley, California 94720, United States; Energy Storage*

and Distributed Resources Division, Lawrence Berkeley National Laboratory, Berkeley, California, 94720, United States

Email: ndantona@berkeley.edu

Shannon W. Boettcher – *Department of Chemistry & Biomolecular Engineering and Department of Chemistry, University of California, Berkeley, California 94720, United States; Energy Storage and Distributed Resources Division, Lawrence Berkeley National Laboratory, Berkeley, California, 94720, United States*

Email: boettcher@berkleley.edu

Author Contributions

The manuscript was written through contributions of all authors. Yang performed the simulations and data analysis. Results and discussion part are largely assisted by D'Antona. Sa conceived and directed the simulation efforts. Boettcher and D'Antona contributed to the manuscript preparation and the formation of the results discussions part. Vincent Briselli and Blaise Daly are acknowledged for the manuscript formatting and proofreading.

Notes

The authors declare no competing financial interest.

ACKNOWLEDGMENTS

The work was funded by the National Science Foundation, Centers for Chemical Innovation Program through Award #2221599 to the Center for Interfacial Ionics. Partial support from the NSF CAREER Award #2047753 is acknowledged.

REFERENCES

(1) Patel, S. K.; Ritt, C. L.; Deshmukh, A.; Wang, Z.; Qin, M.; Epsztein, R.; Elimelech, M. The Relative Insignificance of Advanced Materials in Enhancing the Energy Efficiency of Desalination Technologies. *Energy Environ. Sci.* **2020**, *13* (6), 1694–1710. https://doi.org/10.1039/D0EE00341G.

(2) Epsztein, R.; DuChanois, R. M.; Ritt, C. L.; Noy, A.; Elimelech, M. Towards Single-Species Selectivity of Membranes with Subnanometre Pores. *Nat. Nanotechnol.* **2020**, *15* (6), 426–436. https://doi.org/10.1038/s41565-020-0713-6.

(3) Howorka, S.; Siwy, Z. Nanopore Analytics: Sensing of Single Molecules. *Chem. Soc. Rev.* **2009**, *38* (8), 2360–2384. https://doi.org/10.1039/B813796J.

(4) Chuvilin, A.; Bichoutskaia, E.; Gimenez-Lopez, M. C.; Chamberlain, T. W.; Rance, G. A.; Kuganathan, N.; Biskupek, J.; Kaiser, U.; Khlobystov, A. N. Self-Assembly of a Sulphur-Terminated Graphene Nanoribbon within a Single-Walled Carbon Nanotube. *Nature Mater* **2011**, *10* (9), 687–692. https://doi.org/10.1038/nmat3082.

(5) Zhang, H.; Tian, Y.; Jiang, L. Fundamental Studies and Practical Applications of Bio-Inspired Smart Solid-State Nanopores and Nanochannels. *Nano Today* **2016**, *11* (1), 61–81. https://doi.org/10.1016/j.nantod.2015.11.001.

(6) Zhu, Z.; Wang, D.; Tian, Y.; Jiang, L. Ion/Molecule Transportation in Nanopores and Nanochannels: From Critical Principles to Diverse Functions. *J. Am. Chem. Soc.* **2019**, *141* (22), 8658–8669. https://doi.org/10.1021/jacs.9b00086.

(7) Hou, X.; Guo, W.; Xia, F.; Nie, F.-Q.; Dong, H.; Tian, Y.; Wen, L.; Wang, L.; Cao, L.; Yang, Y.; Xue, J.; Song, Y.; Wang, Y.; Liu, D.; Jiang, L. A Biomimetic Potassium Responsive Nanochannel: G-Quadruplex DNA Conformational Switching in a Synthetic Nanopore. *J. Am. Chem. Soc.* **2009**, *131* (22), 7800–7805. https://doi.org/10.1021/ja901574c.

(8) Tian, Y.; Zhang, Z.; Wen, L.; Ma, J.; Zhang, Y.; Liu, W.; Zhai, J.; Jiang, L. A Biomimetic Mercury(II)-Gated Single Nanochannel. *Chem. Commun.* **2013**, *49* (91), 10679–10681. https://doi.org/10.1039/C3CC42748J.

(9) Guerrette, J. P.; Zhang, B. Scan-Rate-Dependent Current Rectification of Cone-Shaped Silica Nanopores in Quartz Nanopipettes. *J. Am. Chem. Soc.* **2010**, *132* (48), 17088–17091. https://doi.org/10.1021/ja1086497.

(10) Momotenko, D.; Girault, H. H. Scan-Rate-Dependent Ion Current Rectification and Rectification Inversion in Charged Conical Nanopores. *J. Am. Chem. Soc.* **2011**, *133* (37), 14496–14499. https://doi.org/10.1021/ja2048368.

(11) Lan, W.-J.; Edwards, M. A.; Luo, L.; Perera, R. T.; Wu, X.; Martin, C. R.; White, H. S. Voltage-Rectified Current and Fluid Flow in Conical Nanopores. *Acc. Chem. Res.* **2016**, *49* (11), 2605–2613. https://doi.org/10.1021/acs.accounts.6b00395.

(12) White, H. S.; Bund, A. Ion Current Rectification at Nanopores in Glass Membranes. *Langmuir* **2008**, *24* (5), 2212–2218. https://doi.org/10.1021/la702955k.

(13) Choi, Y.; Baker, L. A.; Hillebrenner, H.; Martin, C. R. Biosensing with Conically Shaped Nanopores and Nanotubes. *Phys. Chem. Chem. Phys.* **2006**, *8* (43), 4976–4988. https://doi.org/10.1039/B607360C.

(14) Branton, D.; Deamer, D. W.; Marziali, A.; Bayley, H.; Benner, S. A.; Butler, T.; Di Ventra, M.; Garaj, S.; Hibbs, A.; Huang, X.; Jovanovich, S. B.; Krstic, P. S.; Lindsay, S.; Ling, X. S.; Mastrangelo, C. H.; Meller, A.; Oliver, J. S.; Pershin, Y. V.; Ramsey, J. M.; Riehn, R.; Soni, G. V.; Tabard-Cossa, V.; Wanunu, M.; Wiggin, M.; Schloss, J. A. The Potential and Challenges of

Nanopore Sequencing. *Nat Biotechnol* **2008**, *26* (10), 1146–1153. https://doi.org/10.1038/nbt.1495.
(15) Dekker, C. Solid-State Nanopores. *Nature Nanotech* **2007**, *2* (4), 209–215. https://doi.org/10.1038/nnano.2007.27.
(16) Bayley, H. Nanopore Sequencing: From Imagination to Reality. *Clinical Chemistry* **2015**, *61* (1), 25–31. https://doi.org/10.1373/clinchem.2014.223016.
(17) Howorka, S.; Siwy, Z. S. Nanopores as Protein Sensors. *Nat Biotechnol* **2012**, *30* (6), 506–507. https://doi.org/10.1038/nbt.2264.
(18) Liu, P.; Kong, X.-Y.; Jiang, L.; Wen, L. Ion Transport in Nanofluidics under External Fields. *Chem. Soc. Rev.* **2024**, *53* (6), 2972–3001. https://doi.org/10.1039/D3CS00367A.
(19) Chan, C.; Hsu, J.-P. Rectification Behavior of a Conical Nanopore Subject to Extra Simultaneously Applied Concentration and Thermal Gradients. *Electrochimica Acta* **2023**, *469*, 143208. https://doi.org/10.1016/j.electacta.2023.143208.
(20) He, Y.; Tsutsui, M.; Zhou, Y.; Miao, X.-S. Solid-State Nanopore Systems: From Materials to Applications. *NPG Asia Mater* **2021**, *13* (1), 1–26. https://doi.org/10.1038/s41427-021-00313-z.
(21) Marcuccio, F.; Soulias, D.; Chau, C. C. C.; Radford, S. E.; Hewitt, E.; Actis, P.; Edwards, M. A. Mechanistic Study of the Conductance and Enhanced Single-Molecule Detection in a Polymer–Electrolyte Nanopore. *ACS Nanosci. Au* **2023**, *3* (2), 172–181. https://doi.org/10.1021/acsnanoscienceau.2c00050.
(22) Chen, K.-L.; Yu, R.-J.; Zhong, C.-B.; Wang, Z.; Xie, B.-K.; Ma, H.; Ao, M.; Zheng, P.; Ewing, A. G.; Long, Y.-T. Electrochemical Monitoring of Real-Time Vesicle Dynamics Induced by Tau in a Confined Nanopipette. *Angewandte Chemie International Edition* **2024**, *63* (39), e202406677. https://doi.org/10.1002/anie.202406677.
(23) Ma, H.; Wang, Y.; Li, Y.-X.; Xie, B.-K.; Hu, Z.-L.; Yu, R.-J.; Long, Y.-T.; Ying, Y.-L. Label-Free Mapping of Multivalent Binding Pathways with Ligand–Receptor-Anchored Nanopores. *J. Am. Chem. Soc.* **2024**, *146* (41), 28014–28022. https://doi.org/10.1021/jacs.4c04934.
(24) Chen, K.-L.; Yu, R.-J.; Li, M.-K.; Wang, H.-W.; Xie, B.-K.; Liu, S.-C.; Ying, Y.-L.; Long, Y.-T. In Situ Oxygen Generation via a Platinum-Based Wireless Nanopore Electrode for Single-Cell Manipulation. *Small Methods* **2025**, *9* (5), 2401448. https://doi.org/10.1002/smtd.202401448.
(25) Tagliazucchi, M.; Szleifer, I. Transport Mechanisms in Nanopores and Nanochannels: Can We Mimic Nature? *Materials Today* **2015**, *18* (3), 131–142. https://doi.org/10.1016/j.mattod.2014.10.020.
(26) Ying, Y.-L.; Hu, Z.-L.; Zhang, S.; Qing, Y.; Fragasso, A.; Maglia, G.; Meller, A.; Bayley, H.; Dekker, C.; Long, Y.-T. Nanopore-Based Technologies beyond DNA Sequencing. *Nat. Nanotechnol.* **2022**, *17* (11), 1136–1146. https://doi.org/10.1038/s41565-022-01193-2.
(27) Ramirez, P.; Gomez, V.; Ali, M.; Ensinger, W.; Mafe, S. Net Currents Obtained from Zero-Average Potentials in Single Amphoteric Nanopores. *Electrochemistry Communications* **2013**, *31*, 137–140. https://doi.org/10.1016/j.elecom.2013.03.026.
(28) Xie, X.; Crespo, G. A.; Mistlberger, G.; Bakker, E. Photocurrent Generation Based on a Light-Driven Proton Pump in an Artificial Liquid Membrane. *Nature Chem* **2014**, *6* (3), 202–207. https://doi.org/10.1038/nchem.1858.
(29) Sha, J.; Hasan, T.; Milana, S.; Bertulli, C.; Bell, N. A. W.; Privitera, G.; Ni, Z.; Chen, Y.; Bonaccorso, F.; Ferrari, A. C.; Keyser, U. F.; Huang, Y. Y. S. Nanotubes Complexed with DNA and Proteins for Resistive-Pulse Sensing. *ACS Nano* **2013**, *7* (10), 8857–8869. https://doi.org/10.1021/nn403323k.

(30) Timp, W.; Mirsaidov, U. M.; Wang, D.; Comer, J.; Aksimentiev, A.; Timp, G. Nanopore Sequencing: Electrical Measurements of the Code of Life. *IEEE Trans Nanotechnol* **2010**, *9* (3), 281–294. https://doi.org/10.1109/TNANO.2010.2044418.
(31) Matsui, K.; Goto, Y.; Yanagi, I.; Akahori, R.; Fujioka, M.; Ishida, T.; Yokoi, T.; Nakagawa, T.; Takeda, K. Low-Frequency Noise Induced by Cation Exchange Fluctuation on the Wall of Silicon Nitride Nanopore. *Sci Rep* **2020**, *10* (1), 8662. https://doi.org/10.1038/s41598-020-65530-y.
(32) Liang, S.; Xiang, F.; Tang, Z.; Nouri, R.; He, X.; Dong, M.; Guan, W. Noise in Nanopore Sensors: Sources, Models, Reduction, and Benchmarking. *Nanotechnology and Precision Engineering* **2020**, *3* (1), 9–17. https://doi.org/10.1016/j.npe.2019.12.008.
(33) Lathrop, D. K.; Ervin, E. N.; Barrall, G. A.; Keehan, M. G.; Kawano, R.; Krupka, M. A.; White, H. S.; Hibbs, A. H. Monitoring the Escape of DNA from a Nanopore Using an Alternating Current Signal. *J. Am. Chem. Soc.* **2010**, *132* (6), 1878–1885. https://doi.org/10.1021/ja906951g.
(34) Wu, S.; Ye, W.; Yang, M.; Taghipoor, M.; Meissner, R.; Brugger, J.; Renaud, P. Impedance Sensing of DNA Immobilization and Hybridization by Microfabricated Alumina Nanopore Membranes. *Sensors and Actuators B: Chemical* **2015**, *216*, 105–112. https://doi.org/10.1016/j.snb.2015.03.094.
(35) Nagaraj, V. J.; Jacobs, M.; Vattipalli, K. M.; Annam, V. P.; Prasad, S. Nanochannel-Based Electrochemical Sensor for the Detection of Pharmaceutical Contaminants in Water. *Environ. Sci.: Processes Impacts* **2013**, *16* (1), 135–140. https://doi.org/10.1039/C3EM00406F.
(36) Kitta, K.; Sakamoto, M.; Hayakawa, K.; Nukazuka, A.; Kano, K.; Yamamoto, T. Nanopore Impedance Spectroscopy Reveals Electrical Properties of Single Nanoparticles for Detecting and Identifying Pathogenic Viruses. *ACS Omega* **2023**, *8* (16), 14684–14693. https://doi.org/10.1021/acsomega.3c00628.
(37) Breitsprecher, K.; Janssen, M.; Srimuk, P.; Mehdi, B. L.; Presser, V.; Holm, C.; Kondrat, S. How to Speed up Ion Transport in Nanopores. *Nat Commun* **2020**, *11* (1), 6085. https://doi.org/10.1038/s41467-020-19903-6.
(38) Lewpiriyawong, N.; Yang, C.; Lam, Y. C. Electrokinetically Driven Concentration of Particles and Cells by Dielectrophoresis with DC-Offset AC Electric Field. *Microfluid Nanofluid* **2012**, *12* (5), 723–733. https://doi.org/10.1007/s10404-011-0919-x.
(39) Vaidyanathan, R.; Dey, S.; Carrascosa, L. G.; Shiddiky, M. J. A.; Trau, M. Alternating Current Electrohydrodynamics in Microsystems: Pushing Biomolecules and Cells around on Surfaces. *Biomicrofluidics* **2015**, *9* (6), 061501. https://doi.org/10.1063/1.4936300.
(40) Qiao, L.; Szuttor, K.; Holm, C.; Slater, G. W. Ratcheting Charged Polymers through Symmetric Nanopores Using Pulsed Fields: Designing a Low Pass Filter for Concentrating Polyelectrolytes. *Nano Lett.* **2023**, *23* (4), 1343–1349. https://doi.org/10.1021/acs.nanolett.2c04588.
(41) Fanzio, P.; Manneschi, C.; Angeli, E.; Mussi, V.; Firpo, G.; Ceseracciu, L.; Repetto, L.; Valbusa, U. Modulating DNA Translocation by a Controlled Deformation of a PDMS Nanochannel Device. *Sci Rep* **2012**, *2* (1), 791. https://doi.org/10.1038/srep00791.
(42) Cervera, J.; Schiedt, B.; Neumann, R.; Mafé, S.; Ramírez, P. Ionic Conduction, Rectification, and Selectivity in Single Conical Nanopores. *The Journal of Chemical Physics* **2006**, *124* (10), 104706. https://doi.org/10.1063/1.2179797.
(43) Ma, L.; Li, Z.; Yuan, Z.; Huang, C.; Siwy, Z. S.; Qiu, Y. Modulation of Ionic Current Rectification in Ultrashort Conical Nanopores. *Anal. Chem.* **2020**, *92* (24), 16188–16196. https://doi.org/10.1021/acs.analchem.0c03989.

(44) Liu, Z.; Ma, L.; Zhang, H.; Zhuang, J.; Man, J.; Siwy, Z. S.; Qiu, Y. Dynamic Response of Ionic Current in Conical Nanopores. *ACS Appl. Mater. Interfaces* **2024**, *16* (23), 30496–30505. https://doi.org/10.1021/acsami.4c02078.
(45) Li, C.; Liu, Z.; Qiao, N.; Feng, Z.; Tian, Z. Q. The Electroviscous Effect in Nanochannels with Overlapping Electric Double Layers Considering the Height Size Effect on Surface Charge. *Electrochimica Acta* **2022**, *419*, 140421. https://doi.org/10.1016/j.electacta.2022.140421.
(46) Huang, J.; Pan, X.; Yan, N. Structural Biology and Molecular Pharmacology of Voltage-Gated Ion Channels. *Nat Rev Mol Cell Biol* **2024**, *25* (11), 904–925. https://doi.org/10.1038/s41580-024-00763-7.
(47) Alinezhad, A.; Khatibi, M.; Ashrafizadeh, S. N. Impact of Surface Charge Density Modulation on Ion Transport in Heterogeneous Nanochannels. *Sci Rep* **2024**, *14* (1), 18409. https://doi.org/10.1038/s41598-024-69335-1.
(48) Martinez, J.; Ashby, D.; Zhu, C.; Dunn, B.; Baker, L. A.; Siwy, Z. S. Probing Ion Current in Solid-Electrolytes at the Meso- and Nanoscale. *Faraday Discuss.* **2018**, *210* (0), 55–67. https://doi.org/10.1039/C8FD00071A.
(49) Li, Z.; Bouchal, R.; Mendez-Morales, T.; Rollet, A.-L.; Rizzi, C.; Le Vot, S.; Favier, F.; Rotenberg, B.; Borodin, O.; Fontaine, O.; Salanne, M. Transport Properties of Li-TFSI Water-in-Salt Electrolytes. *J. Phys. Chem. B* **2019**, *123* (49), 10514–10521. https://doi.org/10.1021/acs.jpcb.9b08961.
(50) Ritt, C. L.; De Souza, J. P.; Barsukov, M. G.; Yosinski, S.; Bazant, M. Z.; Reed, M. A.; Elimelech, M. Thermodynamics of Charge Regulation during Ion Transport through Silica Nanochannels. *ACS Nano* **2022**, *16* (9), 15249–15260. https://doi.org/10.1021/acsnano.2c06633.